Microstructure and crystallographic texture of rolled polycrystalline Fe₃Al

D. RAABE, J. KEICHEL
Institut für Metallkunde und Metallphysik, Kopernikusstr. 14, RWTH Aachen, 52056 Aachen, Germany

Z. SUN
Department of Materials Science and Engineering, University of Science and Technology Beijing, 100083 Beijing, People's Republic of China

An imperfectly B_2 ordered Fe₃Al aggregate was cast, thermomechanically hot rolled and finally annealed at 870 K. Subsequently, the specimen was rolled at 800–830 K to a strain ε of 80%. The microstructure and the crystallographic texture of the rolled polycrystalline sample was investigated within the range $\varepsilon = 20$–80%. The microstructure consisted of flat, elongated grains. In numerous grains straight slip lines were detected. Even after $\varepsilon = 80\%$ recrystallization was not observed. The rolling texture of Fe₃Al considerably deviates from that of non-ordered body centered cubic (b.c.c.) alloys and pure b.c.c. metals. The $\{111\}\langle uvw\rangle$ texture fibre (γ-fibre) was very pronounced, while the $\{hkl\}\langle 110\rangle$ fibre (α-fibre) was very weak. The $\{112\}\langle 110\rangle$ orientation which represents the strongest texture component in non-ordered b.c.c. alloys did not occur at all. The textures are discussed in terms of the $\{110\}\langle 111\rangle$, $\{112\}\langle 111\rangle$, $\{112\}\langle 111\rangle$ and $\{123\}\langle 111\rangle$ slip systems. The contribution of crystallographic slip of the various types of potential slip systems was simulated by means of the Taylor theory.

1. Introduction

Intermetallic Fe₃Al based Kurnakov type B_2 ordered alloys [1, 2] have been thoroughly studied in the past due to their technical potential both for low and high temperature applications [3–8] in addition to their excellent oxidation and sulfidation resistance [8–17]. Following the various predicted equilibrium phase diagrams of Fe and Al, Fe₃Al has an imperfectly ordered B_2 (FeAl) structure at temperatures, $T > 823$ K and an ordered DO_3 (Fe₃Al) structure at $T < 823$ K (Fig. 1) [18–23]. However, the B_2 to DO_3 phase transformation is very slow (DO_3 ordering of pure Fe₃Al at 800 K requires about one week) [13–17]. In the presence of ternary additions like Cr, Mo, Zr, Nb, C and B [e.g. 8] the phase transformation to the DO_3 structure may even entirely be suppressed [13–17]. The production of Fe₃Al requires relatively small material costs and the alloy reveals a better strength-to-weight ratio than stainless steels [1–17]. Due to the control of composition and microstructure, corrosion resistance and mechanical properties are considerably improved [1–17], especially room temperature ductility and strength at elevated temperatures.

For elucidating the underlying mechanisms of strength and ductility of plastically deformed Fe₃Al based and comparable B_2 or DO_3 alloys, essentially two methods were applied in the past. First, the influence of antiphase boundary energy was assessed on the selection of slip systems [8, 24–28]. Second, the slip lines on polished sample surfaces were analysed [4, 8, 29].

The interpretation of high temperature deformation experiments on Fe₃Al, which reveals an imperfectly ordered B_2 structure, can be supplemented with comparable examinations on deformed FeAl based samples [28–31]. These investigations indicate that dislocation movement in Fe₃Al based, imperfectly ordered B_2 alloys at elevated temperatures primarily takes place on those glide systems which are typically activated in non-ordered b.c.c. alloys. Additionally, activation of glide systems with a $\langle 100\rangle$ Burger's vector and $\{001\}$ or $\{011\}$ slip planes was predicated [8, 28–31].

In the present study the distribution of grain orientations, hereafter referred to as crystallographic texture, which is developed during warm rolling at $T = 800$–830 K of polycrystalline intermetallic Fe₃Al aggregates, is experimentally investigated using X-ray diffraction [14, 15, 32]. Additionally, the evolution of the microstructure is studied. The application of quantitative textural analysis for the investigation of plastically deformed intermetallic alloys is a useful diagnostic means for two reasons. First, in technical terms the directional behaviour of polycrystalline material is generally an integral property of its
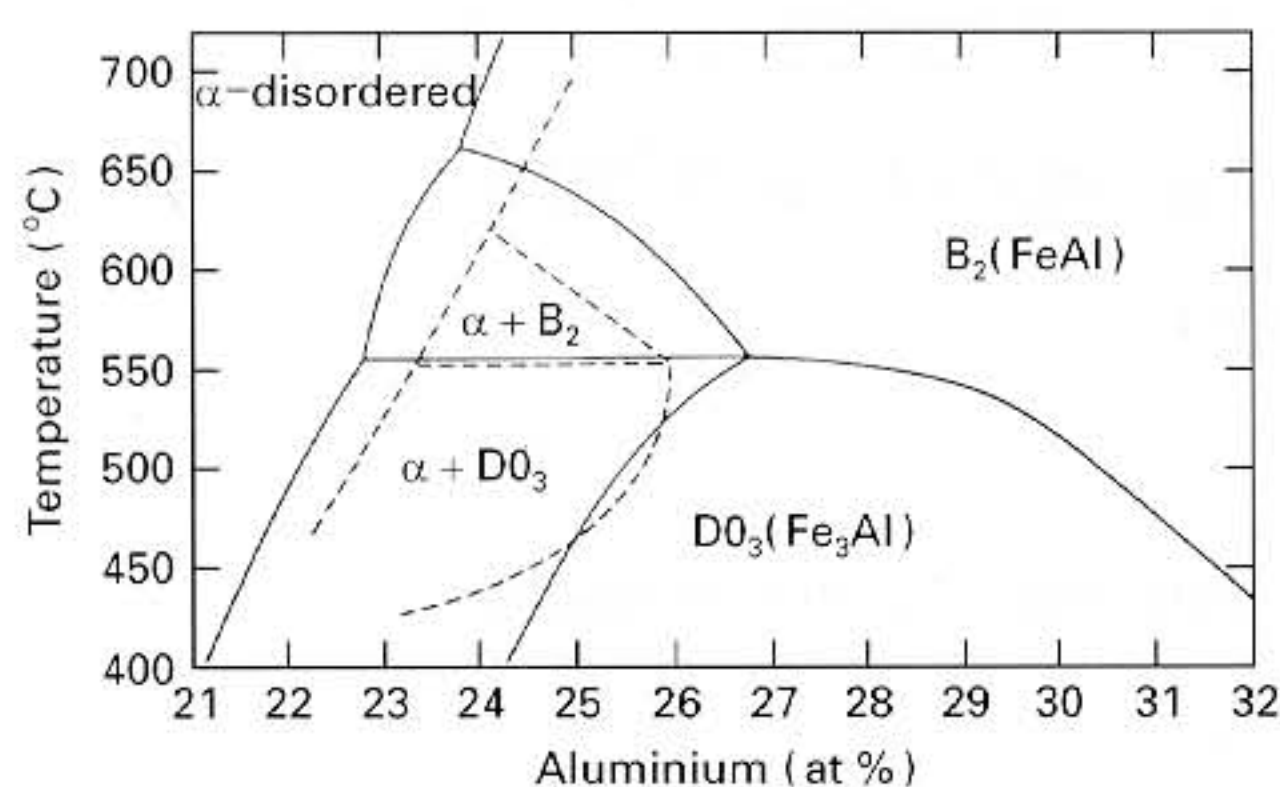
Figure 1 Part of the Fe–Al phase diagram showing the relevant phases [(‒ ‒ ‒) 19, (—) 21].

orientation distribution. Fe_3Al based alloys are considered as potential candidates for applications where stainless steels are nowadays in use. For this reason their directional plastic properties [32], especially their deep drawing behaviour should be investigated. Second, from a more fundamental point of view the development of the orientation distribution during rolling is closely connected to the antisymmetric part of the displacement gradient tensor, which results from the shear imposed by active slip systems. This rigorous geometrical relationship between crystallographic slip and the resulting orientations enables one to use textures as a probe for the determination of slip systems which contribute to plastic deformation.

2. Experimental procedure
2.1. Sample preparation
A cast intermetallic Fe_3Al alloy (Table I) was thermomechanically hot rolled to a final thickness of 4.86 mm [13–17] and finally annealed at 870 K. Subsequently, the sheet was rolled within the temperature range, 800–830 K to $\varepsilon = 80\%$ in a strictly reversing manner, i.e. it was rotated 180° about its transverse direction after each pass. Since homogeneous deformation is primarily determined by the ratio of contact length, l_d, to sheet thickness, d, a ratio of $l < (l_d/d) < 3$ was obtained during cold rolling. According to previous investigations [13–17] and the current X-ray data, the alloy has an imperfectly ordered B_2 structure. Recrystallization was not observed. The microstructure of the rolled samples was studied by means of optical and electron microscopy. For this purpose the specimens were etched in pure HCl (1–3 min) in case of low deformation and in a solution of 10 ml H_2O_2 and 1 ml HF (30 s) in case of heavy deformation ($\varepsilon \geq 70\%$).

2.2. Determination and presentation of crystallographic textures
All texture measurements were carried out in the centre layer of the specimens. The samples were ground and finally etched using pure HCl. The experiments were conducted on an X-ray texture goniometer using $MoK_{\alpha 1}$ radiation. The four incomplete pole figures $\{2\,2\,0\}$, $\{4\,0\,0\}$, $\{4\,2\,2\}$ and $\{6\,2\,0\}$ were measured

within the range of the pole distance angle, $\alpha = 5$–$85°$ in the back reflection mode [33]. From the two-dimensional, centrosymmetric pole figures the quantitative three-dimensional orientation distribution function (ODF) was computed. In earlier investigations the ODFs of intermetallic alloys [32, 34–36] were determined by use of the conventional Fourier type series expansion method [37], which causes mathematical artefacts, referred to as ghost components [38, 39]. These errors, which are attributed to the inversion symmetry of the experimentally achieved pole figures, arise from the absence of the odd order series expansion coefficients. The uncertainties arising from such artefacts usually do not exceed 10% of the texture maximum. The recently introduced iterative series expansion procedure [40–42], however, represents a more reliable method since it generates nearly ghost free ODFs [43]. This method [40–42] which is employed in the present study makes use of two additional assumptions which yield considerable improvements of pole figure inversion as compared to conventional methods [37]. The first ingredient added, referred to as the non-negativity condition, implies that negative pole densities are physically meaningless [40]. The second condition included is the so called "phone concept" [44]. The term "phone" describes an isotropically scattering background texture component [44]. The latter condition increases the non-negativity constraint in such a way that the minimum pole densities of the unmeasured recalculated pole figures are not only set equal to zero but to the pole density of the phone component [41, 42].

In the present investigation a series expansion degree of $l_{max} = 22$ was used. In case of cubic crystal symmetry and orthorhombic sample symmetry an orientation can then be presented by using the three Euler angles $\varphi_1, \phi, \varphi_2$ or the Miller indices $\{h\,k\,l\}\langle u\,v\,w\rangle$. In the latter case the first triple indicates the crystallographic plane parallel to the sheet surface and the second one the crystal vector parallel to the rolling direction (RD). Relevant texture components which are typically generated during rolling of B_2 type aggregates [14, 15, 32] are positioned on the so called α-fibre which comprises all orientations with a common crystallographic $\langle 1\,1\,0\rangle$ direction parallel to RD (e.g. $\{0\,0\,1\}\langle 1\,1\,0\rangle$ at $\phi = 0°$, $\{1\,1\,2\}\langle 1\,1\,0\rangle$ at $\phi \approx 35°$ and $\{1\,1\,1\}\langle 1\,1\,0\rangle$ at $\phi \approx 55°$) and on the so called γ-fibre containing orientations with a common $\{1\,1\,1\}$ plane parallel to the surface of the sheet, i.e. $\{1\,1\,1\}\langle 1\,1\,0\rangle$ at $\varphi_1 = 0°$, 60° and $\{1\,1\,1\}\langle 1\,1\,2\rangle$ at $\varphi_1 = 30°$, 90° (Fig. 2).

3. Results and discussion
Fig. 3a presents the starting texture, i.e. the orientation distribution after casting, thermomechnical hot rolling and final heat treatment. Although the
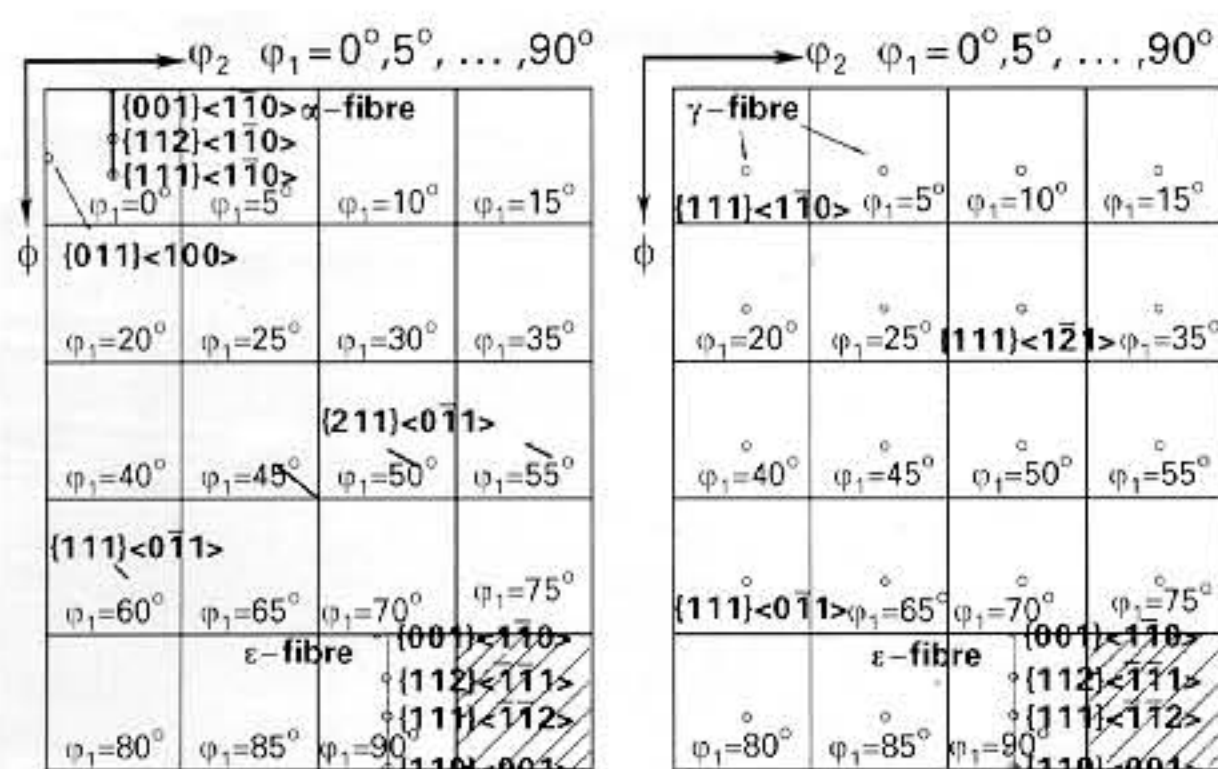
φ₂ φ₁=0°,5°,...,90°   φ₂ φ₁=0°,5°,...,90°

{001}<1̄10> α-fibre				γ-fibre			
{112}<11̄0>							
{111}<11̄0>				{111}<11̄0> φ₁=5°	φ₁=10°	φ₁=15°	
φ₁=0°	φ₁=5°	φ₁=10°	φ₁=15°				
{011}<100>							
φ₁=20°	φ₁=25°	φ₁=30°	φ₁=35°	φ₁=20°	φ₁=25°	{111}<12̄1> φ₁=35°	
		{211}<01̄1>					
φ₁=40°	φ₁=45°	φ₁=50°	φ₁=55°	φ₁=40°	φ₁=45°	φ₁=50°	φ₁=55°
{111}<01̄1>							
φ₁=60°	φ₁=65°	φ₁=70°	φ₁=75°	{111}<01̄1> φ₁=65°	φ₁=70°	φ₁=75°	
ε-fibre	{001}<11̄0>			ε-fibre	{001}<11̄0>		
	{112}<1̄1̄1>				{112}<1̄1̄1>		
	{111}<1̄1̄2>				{111}<1̄1̄2>		
φ₁=80°	φ₁=85°	φ₁=90° {110}<001>		φ₁=80°	φ₁=85°	φ₁=90° {110}<001>	

Figure 2 Typical texture components of rolled intermetallic B₂ ordered alloys [14, 15, 32] and non-ordered b.c.c. metals and alloys [45–48].

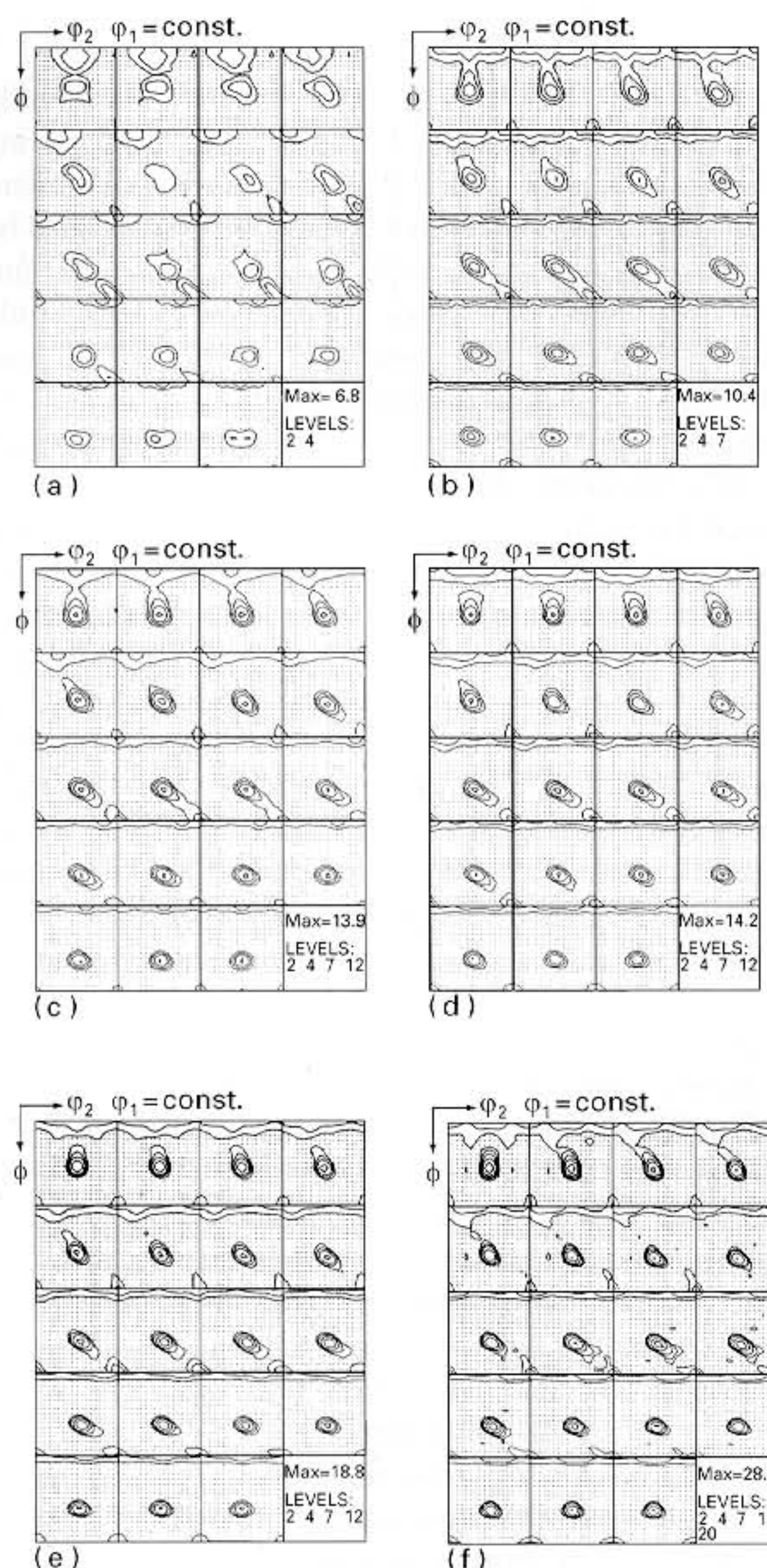φ₂ φ₁=const.   φ₂ φ₁=const.

Max= 6.8
LEVELS: 2 4

(a)

Max=10.4
LEVELS: 2 4 7

(b)

φ₂ φ₁=const.   φ₂ φ₁=const.

Max=13.9
LEVELS: 2 4 7 12

(c)

Max=14.2
LEVELS: 2 4 7 12

(d)

φ₂ φ₁=const.   φ₂ φ₁=const.

Max=18.8
LEVELS: 2 4 7 12

(e)

Max=28.4
LEVELS: 2 4 7 12 20

(f)

Figure 3 Experimentally detected rolling textures (T_{roll} = 800–830 K), orientation distribution function calculated by use of the iterative series expansion method (l_{max} = 22) [40–42]. Presentation in φ_1 sections: (a) ε = 0%, (b) ε = 20%, (c) ε = 30%, (d) ε = 50%, (9e) ε = 60%, and (f) ε = 80%.

maximum occurring orientation density is quite small, $f(g)_{max}$ = 6.8, the ODF reveals two main components, one close to {1 1 2}⟨1 1 0⟩ and a second one close to {0 0 1}⟨1 1 0⟩. Additionally, a weak γ-fibre appears. In
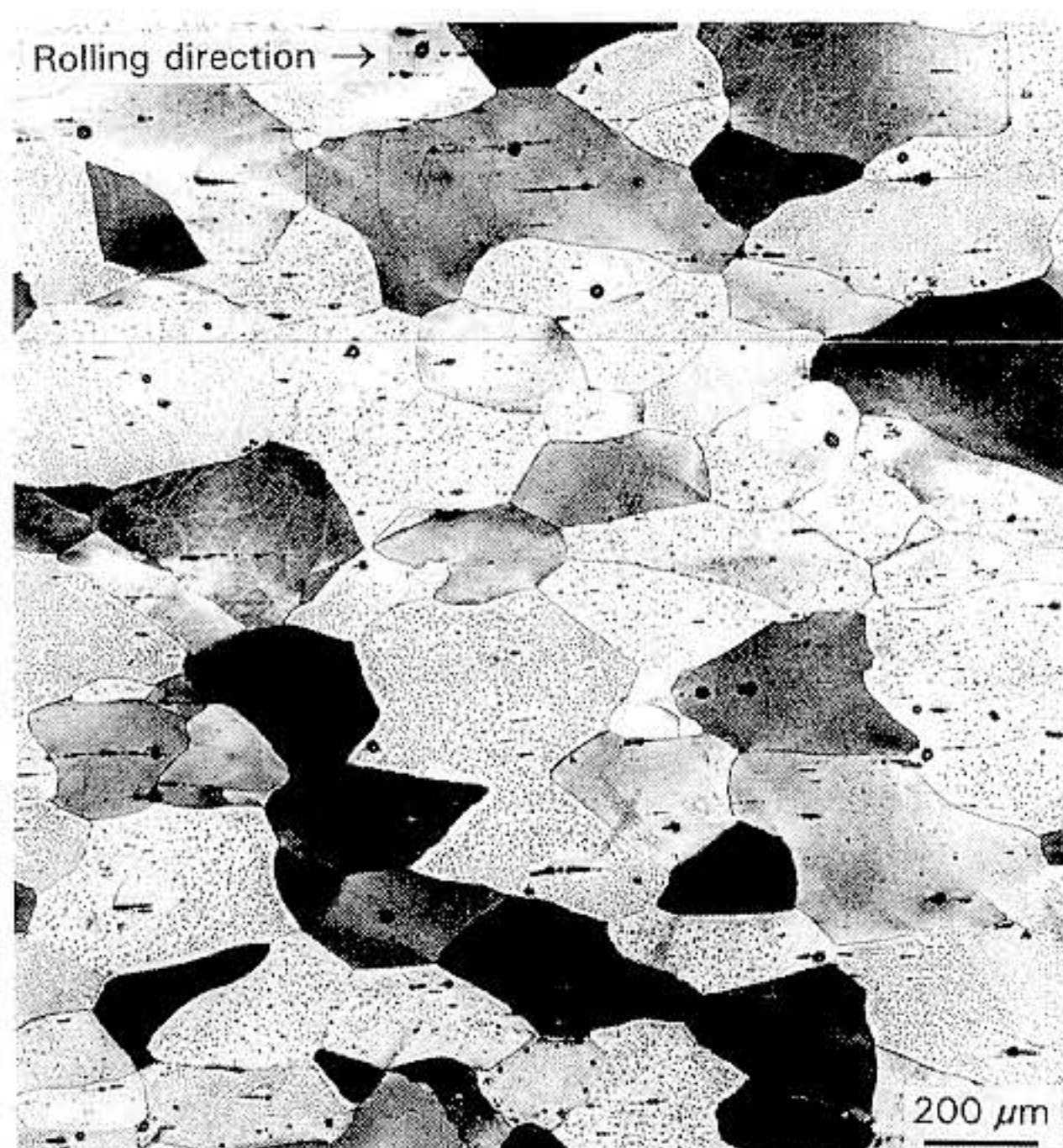
Rolling direction →

200 μm

Figure 4 Longitudinal section of the material after casting, thermomechanical hot rolling and subsequent annealing at 870 K.

the longitudinal section the corresponding microstructure (Fig. 4) reveals nearly equiaxed grains which indicates that recrystallization has taken place during or subsequent to the thermomechanical treatment.

After 20% rolling deformation the texture reveals a dominant component close to {1 1 1}⟨1 1 0⟩ on the α-fibre and an orientation tube close to the γ-fibre (Fig. 3b). Furthermore, a weak {0 0 1}⟨u v w⟩ texture fibre appears. With increasing rolling deformation, ε = 30% (Fig. 3c) and ε = 50% (Fig. 3d), the γ-fibre gradually increases. The orientation density of the {0 0 1}⟨u v w⟩ texture fibre, especially of the {0 0 1}⟨1 1 0⟩ component remains very weak when compared to the maximum occurring orientation density on the γ-fibre (Fig. 3c, d). The formation of a {1 1 1}⟨u v w⟩ texture fibre consisting of a strong {1 1 1}⟨1 1 0⟩ and {1 1 1}⟨1 1 2⟩ orientation is well known from cold rolled non-ordered b.c.c. alloys [45–48]. However, in such materials the γ-fibre is accompanied by an α-fibre, especially by a {0 0 1}⟨1 1 0⟩ and a strong {1 1 2}⟨1 1 0⟩ component. The rolled Fe₃Al specimen reveals a weak {0 0 1}⟨1 1 0⟩ orientation, but the {1 1 2}⟨1 1 0⟩ component does not appear at all. Although the latter orientation was present in the initial texture (Fig. 3a), it decreases during subsequent cold rolling rather than stabilizes (Fig. 3b–d). The longitudinal sections of the corresponding microstructures (Figs 5 and 6) reveal the development of an elongated and equiaxed grain morphology. Mesoscopic morphological phenomena, such as shear banding or grain fragmentation, which usually indicate instable deformation were not observed. The deformation microstructure of polycrystalline Fe₃Al is similar to pure b.c.c. metals and weakly alloyed non-ordered b.c.c. materials.

The rolling textures observed after low strains (Fig. 3b–d) are stabilized after higher degrees of deformation, ε = 60% (Fig. 3e) and 80% (Fig. 3f). The

341

Rolling direction →
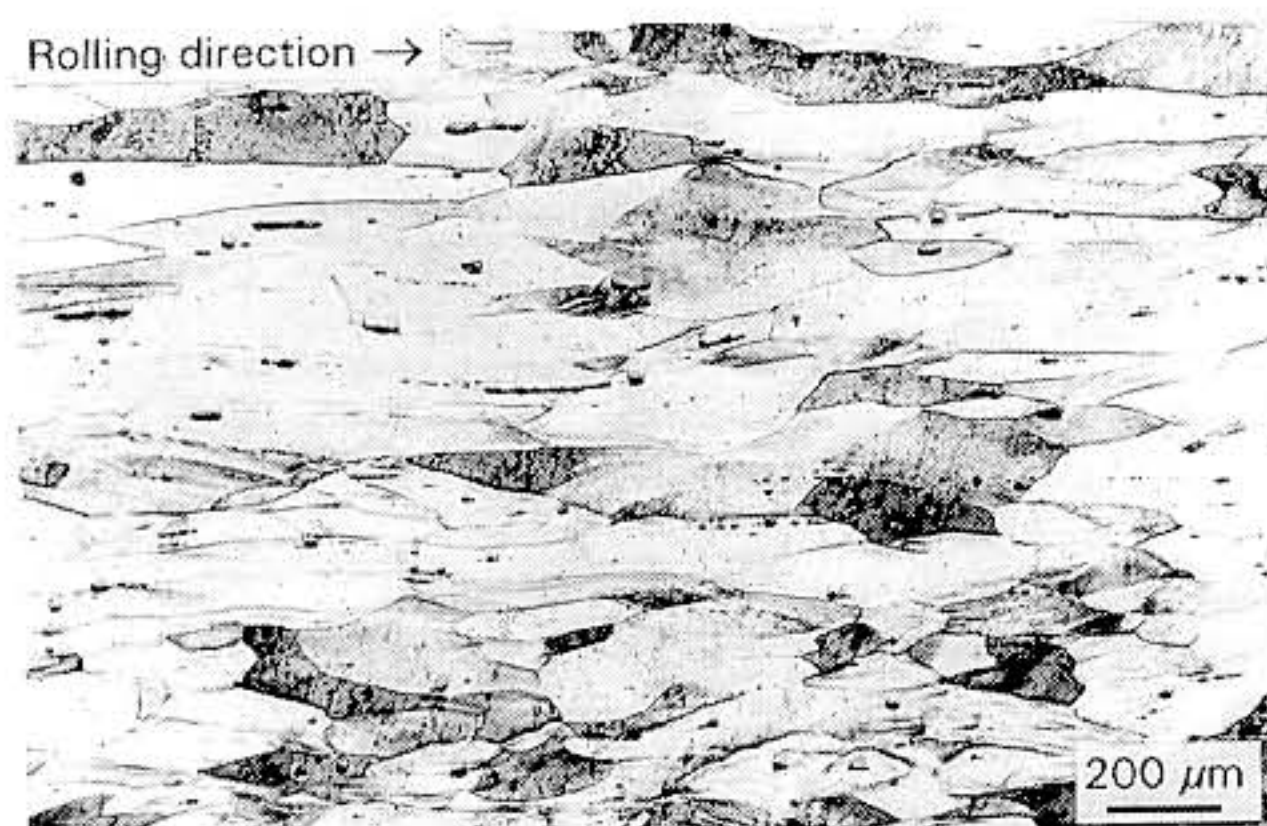

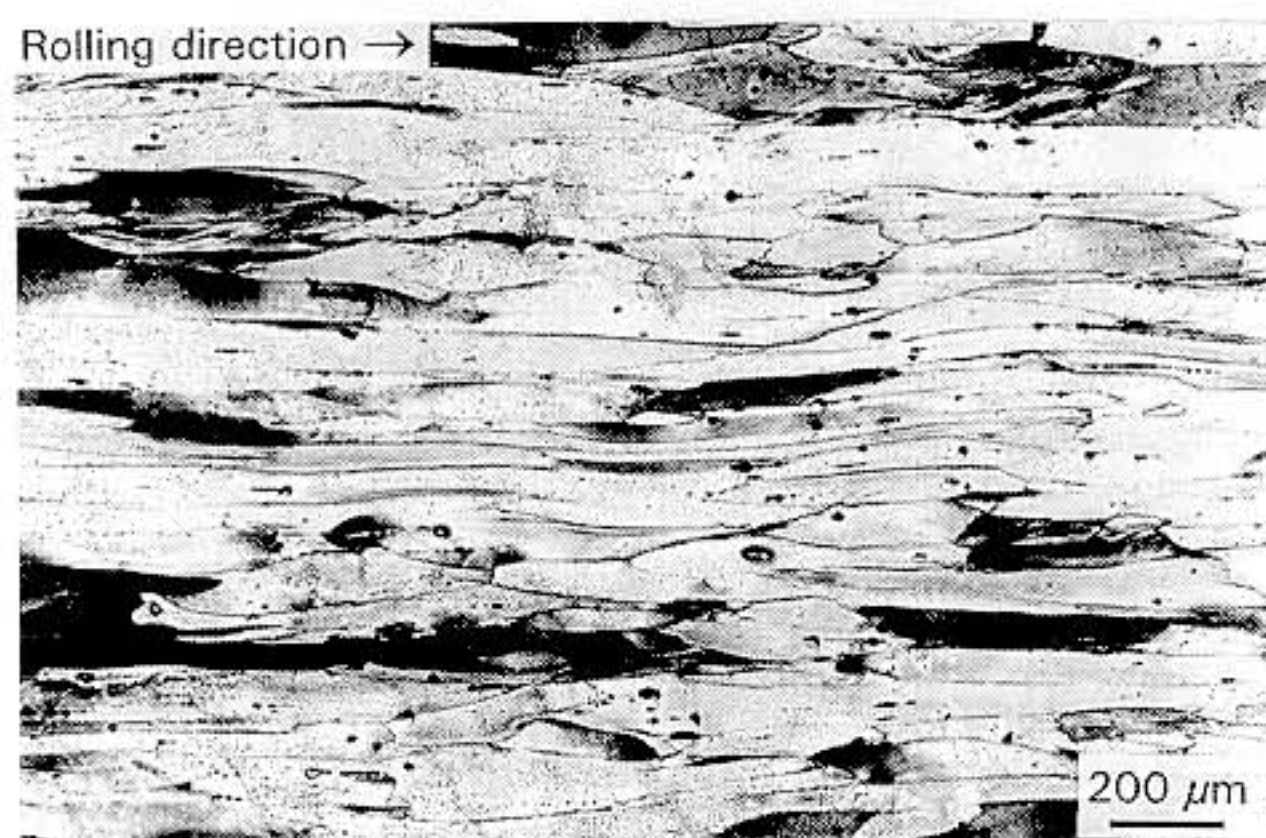*Figure 5* Longitudinal section after 20% rolling deformation at 800–830 K.

Rolling direction →

Figure 6 Longitudinal section after 30% rolling deformation at 800–830 K.

orientation density of the γ-fibre increases while the {0 0 1}⟨1 1 0⟩ component remains very weak. However, the {1 1 2}⟨1 1 0⟩ orientation does not appear at all (Fig. 3e, f). Also after large strains the microstructure is very similar to that of heavily cold rolled non-ordered b.c.c. alloys.

Slip lines were noticed in the longitudinal sections of many grains (Fig. 7). These lines were usually straight rather than wavy and often only one or two types of slip lines were observed (Fig. 7). Such slip line patterns are somewhat different from those reported for pure b.c.c. metals or non-ordered b.c.c. alloys [49, 50]. Since b.c.c. metals do not contain close packed crystallographic planes they reveal three types of potential glide planes generating 12 {1 1 0}⟨1 1 1⟩, 12 {1 1 2}⟨1 1 1⟩ and 24 {1 2 3}⟨1 1 1⟩ slip systems. Since cross slip is not intrinsically hindered in b.c.c. metals their slip lines often have a wavy rather than a straight shape. The only well known exception is Fe with an Si content of about 3 wt % where slip is restricted to the 12 {1 1 0}⟨1 1 1⟩ systems. Consequently, in Fe–3 wt % Si slip lines appear straight rather than wavy [49, 50]. Although in the alloy under investigation the slip lines were also straight this does not necessarily mean that dislocation movement is restricted to {1 1 0} planes. It must be considered that straight slip lines may indicate either that cross slip is simply impeded or that one type of slip system prevails during deformation.

However, additional conclusions may be drawn from the slip line observations and deformation tex-
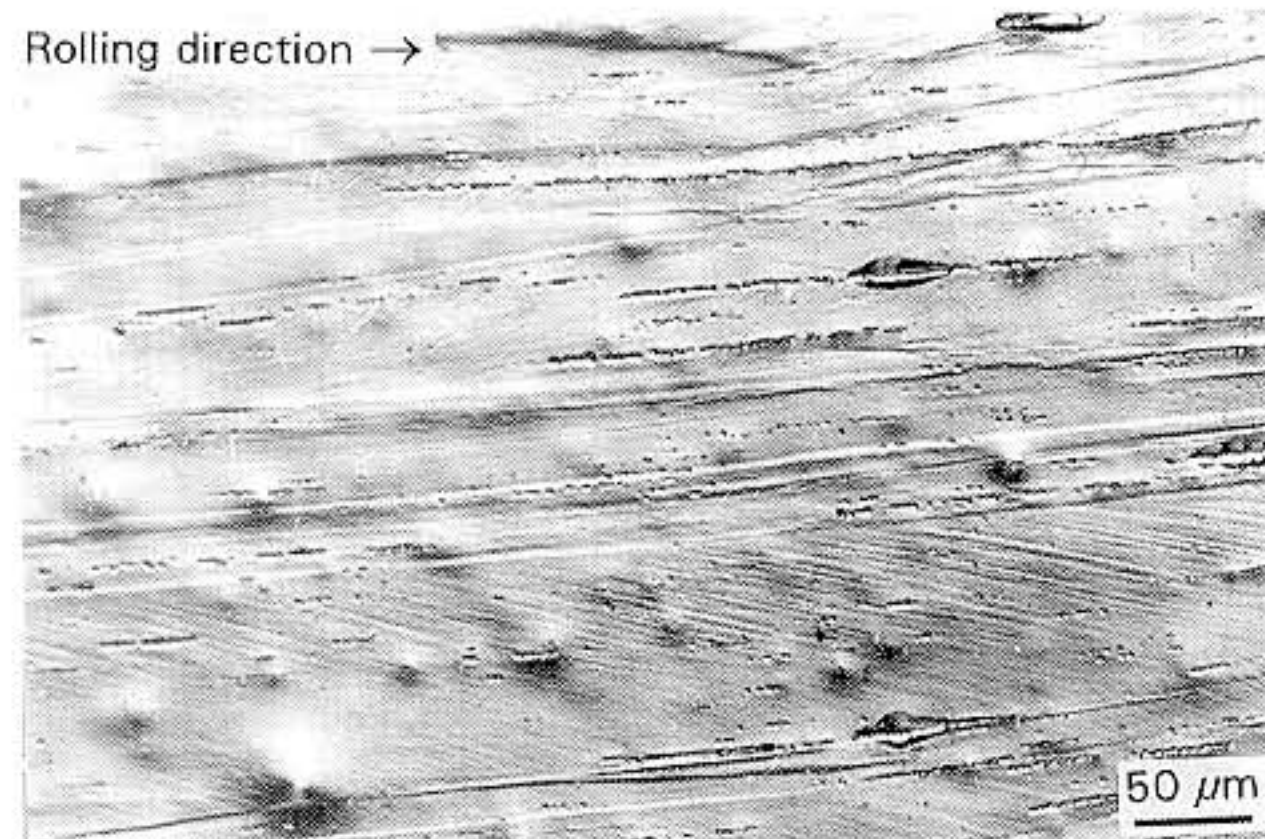
Rolling direction →

Figure 7 Longitudinal section after 80% rolling deformation at 800–830 K. In numerous grains straight slip lines were observed.

tures. If {1 1 0}⟨1 1 1⟩ slip systems had dominantly contributed to plastic deformation of Fe_3Al during rolling, a strong {1 1 2}⟨1 1 0⟩ texture component would have been generated. This is well established by numerous experiments and Taylor type simulations on non-ordered b.c.c. alloys [e.g. 45–48]. This would also be true in the case that {1 1 2}⟨1 1 1⟩ and {1 2 3}⟨1 1 1⟩ had accompanied slip on {1 1 0}⟨1 1 1⟩ systems [32]. The {1 1 2}⟨1 1 0⟩ orientation which usually represents the maximum texture component of rolled b.c.c. alloys [45–48] was, however, not found in the rolled Fe_3Al specimens. In non-ordered b.c.c. aggregates there are only two ways to avoid the strong {1 1 2}⟨1 1 0⟩ orientation. First, the externally imposed deformation tensor can be modified [47], e.g. torsion or cross rolling instead of rolling deformation under plane strain conditions, and second, the grain morphology can be discontinuously modified by recrystallization of the rolled specimen. However, neither case applies in the present situation.

Since the crystallographic texture is closely connected with the activated slip systems [51–57] it may be concluded that {1 1 0}⟨1 1 1⟩ slip systems only play a minor role for the plastic deformation of Fe_3Al polycrystals. This assumption is confirmed by a Taylor type model. Simulations according to Taylor [53] are based on the description of macroscopic deformation by means of crystallographic slip. The macroscopic deformation is characterized by the displacement gradient tensor written in lattice co-ordinates. Its symmetric part represents the strain tensor, while the antisymmetric part describes the resulting plastic rigid body rotation (not the grain rotation). From the latter tensor and the displacement gradient tensor written in machine co-ordinates the relevant orientation changes can be computed [e.g. 54]. The macroscopic deformation during rolling consists of elongation in rolling direction and thickness reduction parallel to the sheet plane normal (ideal plane strain tensor). In the so called full constraints Taylor approach [53] the imposed strain tensor is transferred into each grain where it is fulfilled by crystallographic slip. Consequently, compatibility of the grains during deformation is included.
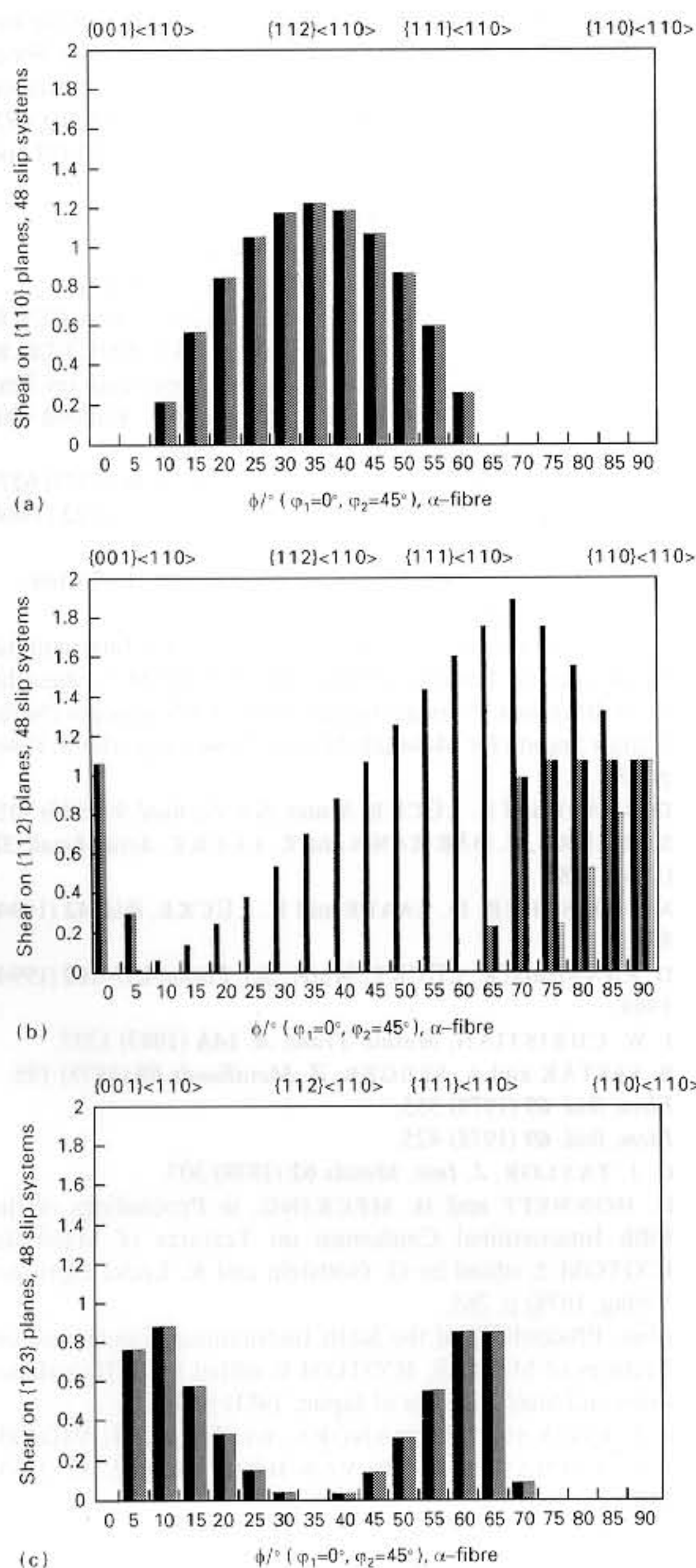
{001}<110> {112}<110> {111}<110> {110}<110>

(a) $\phi/°\ (\varphi_1=0°, \varphi_2=45°),\ \alpha$–fibre

{001}<110> {112}<110> {111}<110> {110}<110>

(b) $\phi/°\ (\varphi_1=0°, \varphi_2=45°),\ \alpha$–fibre

{001}<110> {112}<110> {111}<110> {110}<110>

(c) $\phi/°\ (\varphi_1=0°, \varphi_2=45°),\ \alpha$–fibre

Figure 8 Simulated shear contribution of the three types of potential b.c.c. slip systems in grains with α-fibre orientation. Taylor type simulations [53–57] including all 48 potential b.c.c. slip systems [49, 50–52] (12{110}$\langle 111 \rangle$, 12{112}$\langle 111 \rangle$ and 24 {123}$\langle 111 \rangle$ systems) with identical critical resolved shear stress. Each column represents the amount of shear contributed by a single slip system: Contribution of (a) {110}$\langle 111 \rangle$ slip systems, (b) {112}$\langle 111 \rangle$ slip systems, and (c) {123}$\langle 111 \rangle$ slip systems.

From the above it follows that various types of information can be extracted from Taylor simulations, namely the types and the shear contributions of the active slip systems and the resulting grain rotations. Typically, the latter information is used [32, 34, 36]. However, in this study the individual shear contribution of each type of active glide system is investigated. In the present simulation all three types of b.c.c. slip systems, i.e. {110}$\langle 111 \rangle$ (12), {112}$\langle 111 \rangle$ (12) and {123}$\langle 111 \rangle$ (24) are used. Fig. 8 presents the shear contributed by each type of slip system for main orientations on the α-fibre. Fig. 8a presents the shear on {110}$\langle 111 \rangle$, Fig. 8b that on {112}$\langle 111 \rangle$ and Fig. 8c that on {123}$\langle 111 \rangle$ glide systems. Each column represents the amount of shear contributed by a single slip system. The simulation shows that {110}$\langle 111 \rangle$ systems (Fig. 8a) mainly contribute to the stabilization of the {112}$\langle 110 \rangle$ texture component ($\phi = 35°$). Their contribution to the stabilization of the {111}$\langle 110 \rangle$ ($\phi \approx 55°$) component, however, is negligible.

In a previous investigation similar simulation techniques were employed [32]. The study which was carried out on rolled Fe_3Al with 2 at % Cr content showed that glide systems with a $\langle 100 \rangle$ Burger's vector and {001} or {011} slip planes which were found in deformed single crystals [8, 28–31] did not contribute to the plastic deformation in polycrystalline Fe_3Al.

Neglecting hence both {110}$\langle 111 \rangle$ and cubic slip systems, only the {112}$\langle 111 \rangle$ and {123}$\langle 111 \rangle$ systems remain. The Taylor type simulations suggest that one {112}$\langle 111 \rangle$ (Fig. 8b) as well as two {123}$\langle 111 \rangle$ glide systems (Fig. 8c) contribute to the formation and stabilization of the {111}$\langle 110 \rangle$ orientation ($\phi \approx 55°$). However, the current results do not clearly show whether the {112}$\langle 111 \rangle$ or the {123}$\langle 111 \rangle$ glide systems prevail.

4. Conclusions

The development of texture and microstructure during rolling of a B_2 ordered polycrystalline Fe_3Al aggregate was studied within the range $\varepsilon = 20$–80%. The rolling textures revealed a strong {111}$\langle uvw \rangle$ texture fibre. The {001}$\langle 110 \rangle$ component was very weak. The {112}$\langle 110 \rangle$ orientation which was present in the starting texture decreased rather than stabilized during rolling. These results were compared to cold rolling textures of non-ordered b.c.c. alloys and to Taylor simulations by which the shear contribution of the various types of slip systems was computed. This comparison indicated that plastic deformation of Fe_3Al polycrystals is essentially accomplished by slip on {112}$\langle 111 \rangle$ and possibly also on {123}$\langle 111 \rangle$ systems. However, the contribution of {110}$\langle 111 \rangle$ and cubic glide systems seemed to play a minor role. Slip lines were discovered in numerous grains. However, these lines were not wavy as in non-ordered b.c.c. alloys, but straight. This observation indicated that either cross slip is impeded or that one type of slip system prevails during deformation of Fe_3Al.

References

1. N. ZIEGLER, *Trans AIME* **100** (1932) 267.
2. C. SYKES and J. BAMPFYLDE, *J. Iron Steel Inst.* **130** (1934) 389.
3. R. G. DAVIES, *J. Phys. Chem. Solids* **24** (1963) 985.
4. N. S. STOLOFF and R. G. DAVIES, *Acta Metall.* **12** (1964) 473.
5. H. J. LEAMY, E. D. GIBSON and F. X. KAYSER, *ibid.* **15** (1967) 1827.
6. H. J. LEAMY and F. X. KAYSER, *Phys. Status Solidi* **34** (1969) 765.
7. H. J. LEAMY, *Acta Metall.* **15** (1967) 1839.
8. C. G. MCKAMEY, J. H. DE VAN, P. F. TORTORELLI and V. K. SIKKA, *J. Mater. Res.* **6** (1991) 1779.

9. P. TOMASZEWICZ and G. R. WALLWORK, *Rev. High Temp. Mater.* **4** (1978) 76.
10. *Idem, Oxid. Metall.* **19** (1983) 165.
11. F. A. GOLIGHTLY, F. H. STOTT and G. C. WOOD, *ibid.* **10** (1976) 163.
12. P. FOX and G. J. TATLOCK, *Mater. Sci. Technol.* **4** (1988) 439.
13. Z. SUN, Y. HUANG, W. YANG and G. CHEN, in "High Temperature Ordered Intermetallic Alloys V", edited by I. Baker, R. Darolia, J. D. Whittenberger and M. Yoo, Materials Research Symposium Proceedings, Pittsburgh, Vol. 288, 1992 (Materials Research Society, 1993) p. 885.
14. W. MAO and Z. SUN, *Scripta Metall.* **29** (1993) 217.
15. W. MAO and Z. SUN, *Mater. Sci. Forum* **157–162** (1994) 1009.
16. G. CHEN, Y. HUANG, W. YANG and Z. SUN, in Proceedings of the Conference of Processes, Properties and Applications of Iron Aluminides (Triple M's Societies, Warrendale, PA, 1994) p. 3.
17. Z. SUN, Y. HUANG, W. YANG and G. CHEN, in Proceedings of the Conference of High Temperature Properties of Iron based Aluminides (Triple M's Societies, San Francisco, CA, 1994) p. 3.
18. T. B. MASALSKI, "Binary Alloy Phase Diagrams" (American Society for Metals, Metals Park, OH, 1986).
19. K. OKI, M. HASAKA and T. EGUCHI, *Jpn. J. Appl. Phys.* **12** (1973) 1522.
20. P. R. SWANN, W. R. DUFF and R. M. FISHER, *Trans. AIME* **245** (1969) 851.
21. H. OKAMOTO and P. A. BECK, *Metall. Trans.* **2** (1971) 569.
22. S. M. ALLEN and J. W. CAHN, *Acta Metall.* **23** (1975) 1017.
23. *Idem, ibid.* **24** (1976) 425.
24. W. A. RACHINGER and A. H. COTTRELL, *ibid.* **4** (1956) 109.
25. S. TAKEUCHI, in Fifth International Conference on Strength of Metals and Alloys, edited by P. Haasen, V. Gerold and G. Kostorz (Aachen, 1979) p. 53.
26. Y. UMAKOSHI, *Mater. Sci. Technol.* **6** (1993) 251.
27. Y. UMAKOSHI and M. YAMAGUCHI, *Phil. Mag.* **A41** (1980) 573.
28. *Idem, ibid.* **A44** (1981) 711.
29. M. J. MARCINKOWSKI and N. BROWN, *Acta. Metall.* **9** (1961) 764.
30. I. BAKER and D. J. GAYDOSH, *Mater. Sci. Engng* **96** (1987) 147.
31. *Idem, Phys. Status Solidi* **96** (1986) 185.
32. D. RAABE and W. MAO, *Phil. Mag.* **A71** (1995) 805.
33. L. G. SCHULZ, *J. Appl. Phys.* **20** (1949) 1030.
34. D. RAABE, D. PONGE and B. STOLZ, in Proceedings of the 15th Riso International Symposium on Materials Science, Numerical Prediction of Defomation Proceeding and the Behaviour of Real Materials, edited by S. I. Andersen, J. B. Bilde-Sorensen, T. Lorentzen, O. B. Pedersen and N. J. Sorensen (RISO National Laboratory, Roskilde, Denmark, 1994) p. 493.
35. J. BALL and G. GOTTSTEIN, *Intermetallics* **1** (1993) 171 and 191.
36. D. RAABE, *Acta Metall.* **43** (1995) 1531.
37. H. J. BUNGE, *Z. Metallunde* **56** (1965) 872.
38. S. MATTHIES, *Phys. Status Solidi (b)* **98** (1980) K113.
39. H. R. WENK, H. J. BUNGE J. KALLEND, K. LÜCKE, S. MATTHIES, J. POSPIECH and P. VAN HOUTTE, in Proceedings of the Eighth International Conference on Textures of Materials, ICOTOM 8, edited by J. Kallend and G. Gottstein (The Metallogical Society, 1988) p. 17.
40. H. J. BUNGE and C. ESLING, *J. Phys. Lett.* **40** (1979) 627.
41. M. DAHMS and H. J. BUNGE, *J. Appl. Crystallog.* **22** (1989) 439.
42. M. DAHMS, *Textures and Microstructures* **19** (1992) 169.
43. D. RAABE, *ibid.* **23** (1995) 115.
44. S. MATTHIES, in Proceedings of the Seventh International Conference on Textures of Materials, ICOTOM 7, edited by C. M. Brakman, P. Jongenburger and E. J. Mittenseijer (Netherlands Society for Materials Science, Noordwijkerhout, 1984) p. 737.
45. D. RAABE and K. LÜCKE, *Mater. Sci. Technol.* **9** (1993) 302.
46. S. MISHRA, C. DÄRMANN and K. LÜCKE, *Acta Metall.* **32** (1984) 2185.
47. M. HÖLSCHER, D. RAABE and K. LÜCKE, *ibid.* **42** (1994) 879.
48. D. RAABE and K. LÜCKE, *Mater. Sci. Forum* **157–162** (1994) 1969.
49. J. W. CHRISTIAN, *Metall. Trans. A.* **14A** (1983) 1237.
50. B. SESTÁK and A. SEEGER, *Z. Metallunde* **69** (1978) 195.
51. *Idem, ibid.* **69** (1978) 355.
52. *Idem, ibid.* **69** (1978) 425.
53. G. I. TAYLOR, *J. Inst. Metals* **62** (1938) 307.
54. H. HONNEFF and H. MECKING, in Proceedings of the Fifth International Conference on Textures of Materials, ICOTOM 5, edited by G. Gottstein and K. Lücke (Springer Verlag, 1978) p. 265.
55. *Idem*, Proceedings of the Sixth International Conference on Textures of Materials, ICOTOM 6, edited by S. Nagashima (Iron and Steel Institute of Japan, 1981) p. 347.
56. U. F. KOCKS and H. CHANDRA, *Acta Metall.* **30** (1982) 695.
57. J. L. RAPHANEL and P. VAN HOUTTE, *ibid.* **33** (1985) 1481.